www.czasopisma.pan.pl PAN POLSKA AKADEMIA NAUK www.journals.pan.pl
Chemical and Process Engineering 2013, 34 (1), 87-100
DOI: 10.2478/cpe-2013-0008

MODELLING THE DYNAMICS OF FLEXIBLE AND RIGID FIBRES

Grzegorz Kondora*, Dariusz Asendrych

Czestochowa University of Technology, Institute of Thermal Machinery, 42-200 Czestochowa, Poland

A particle-level simulation technique has been developed for modelling fibre suspension flow in a converging channel of a papermachine headbox. The fibre model is represented by a chain of elements connected together. The model was verified by the simulation of rigid fibre dynamics in a simple shear flow. The period of rotation was found to be in a very good agreement with theory and reference data. The model was then employed to simulate fibre motion in a converging channel of a papermachine headbox. Fibre suspension motion was resolved using two-step procedure. Velocity field was calculated by means of a commercial CFD code ANSYS Fluent with RSM turbulence model applied and used as an input to the in-house code allowing to simulate fibre dynamics. Results of the calculations were used to construct the fibre orientation probability distribution (FOPD) which was found to be consistent with available experimental data.

Keywords: fibre dynamics, fibre orientation, Lagrange method, particle-level simulation, headbox flow

1. INTRODUCTION

Multiphase flows with fibrous particles may be found in various industrial processes, just to mention production of polymers, insulation materials or biomass combustion. Papermaking industry is one of those in which fibres are present at almost all stages of a product life.

Paper is produced from pulp suspension consisting of water, cellulose fibres and some chemical additives. Basic paper structure is formed in the so called headbox - specially shaped duct being the first part of the papermachine. It was confirmed by many research studies that flow phenomena occurring in a headbox have a great influence on the end product properties (e.g. Jetsu et al., 2001). For instance an uneven mass distribution of suspension in a sheet may lead to dimensional stability problems such a paper cockling and curling (see e.g. Leppanen, 2007). Depending on the desired paper properties, fibres in a flowing suspension should be properly oriented both in machine direction (MD) and in cross direction (CD), thus controlling and understanding wet end flow conditions is of great importance.

Very serious difficulties with measuring and characterising pulp suspension may be encountered during experiments, mainly because of the non-homogenous nature of the medium, i.e. its strong multiphase character, non-transparency, non-Newtonian behaviour etc. That is why papermaking is one of industrial sectors requiring coupled numerical modelling with experimental measurements to ensure further development.

Great effort has been made for describing the dynamical behaviour of non-spherical particles in various flow fields. Jeffery (1922) derived equations for the motion of inertia-less, rigid, ellipsoidal particles

*Corresponding author, e-mail: kondora@imc.pcz.czest.pl

immersed in a Stokes flow of a Newtonian fluid. Complex mathematical analysis performed by Jeffery showed that the period of rotation is a function of aspect ratio and a shear rate and also that the orbit depends on the initial orientation of the ellipsoid relative to the shear plane. Many other researchers (e.g. Batchelor, 1970; Brenner, 1964; Bretherton, 1962) have extended Jeffery's theory to arbitrary particle shapes.

During the last decades many researchers have been developing numerical models by means of Euler-Lagrange approach. Yamamoto and Matsuoka (1993) have proposed a method for simulating the dynamic behaviour of both rigid and flexible fibres in a flow field. The model consisting of spheres connected by springs could simulate stretching, bending and twisting. The authors found the period of rotation and distribution of orientation angle calculated from simulations to be in a good agreement with those from the Jeffery's theory. Elsewhere (Yamamoto and Matsuoka, 1993; 1994) equations of motion were solved for every constituent particle without applying constraints between adjacent segments. Integrity of the fibre has been maintained by means of stretching force applied between adjacent segments. Fibres were suspended in a prescribed shear flow and a low particle Reynolds number was assumed. In the later papers Yamamoto and Matsuoka (1994; 1999) introduced a repulsive potential force (having exponential character) to prevent overlapping bead surfaces.

Schmid et al. (2000) as well as Ross and Klingenberg (1997) modelled single fibre as a chain of interconnected rods instead of using spherical beads. Constraint force was included but the model was limited to very low Reynolds numbers (Stokes flow assumption). A comprehensive fibre model developed by Lindström and Uesaka (2008) was applied to study sheet formation phenomena occurring in a forming section of a papermachine. The authors found Lagrangian simulation technique to be very useful in modelling fibre suspension flow, especially when a detailed look at individual fibres is needed, e.g. fibre orientation or flock formation process.

2. FIBRE MODEL

2.1. General fibre model

Fibre is modelled as a chain of N_{seg} rigid segments connected by ball and socket joints. Different geometrical objects (see Fig. 1) may be used to represent fibre segments, for example: cylinders, prolate spheroids, or in the simplest case, spheres.

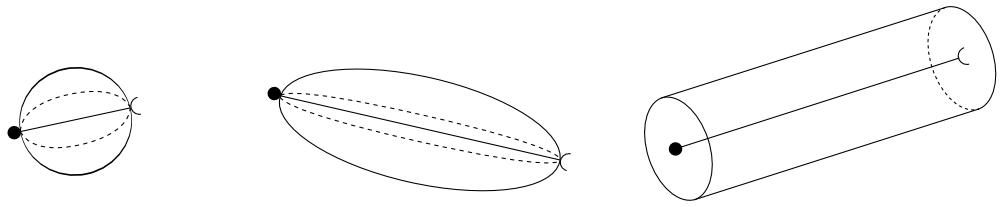

Fig. 1. A sphere, prolate spheroid and cylinder representing fibre segment

Every segment is uniquely described by a set of parameters: index i [1,N_{seg}], centre-of-mass position $\mathbf{r}_i$, normalised direction vector $\mathbf{z}_i$ in a local right-hand coordinate system Γ_i (see Fig. 2) attached to the segment. Segment i has two joints – J_i and J_{i+1}. Obviously hinges No. J_1 and J_{Nseg+1} are virtual since they are not connected to any others.

Equations of motion in the Cartesian coordinate system are derived from force and torque balances for each segment. In order to maintain fibre integrity an additional constraint equation is required to close the system. Balances contain contributions from different sources: hydrodynamic force and torque,

elastic bending and twisting torque, inter-fibre and fibre-wall collisions. Main forces and torques acting on a fibre consisting of rigid cylinders are illustrated in Fig. 3.

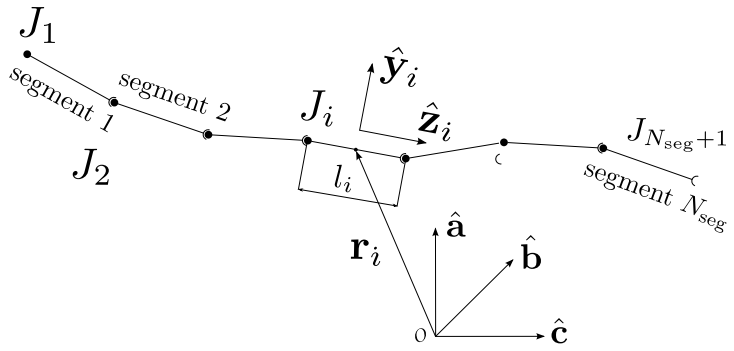

Fig. 2. Fibre model consisting of N_{seg} segments connected by ball and socket joints

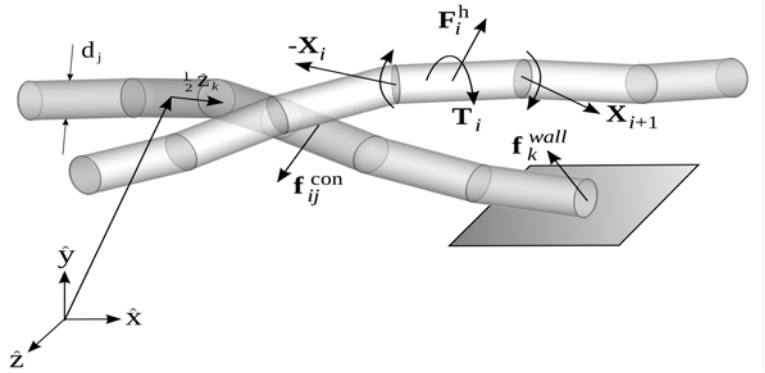

Fig. 3. Main forces and torques acting on a fibre

Neglecting Brownian motion direct application of Newton's second law for a fibre's i^{th} segment leads to:

$$m_i\dot{\mathbf{r}}_i = \mathbf{F}_i^h + \mathbf{F}_i^w + \sum_j \mathbf{f}_{ij}^{con} + \mathbf{f}_i^{wall} - \mathbf{X}_{i+1} + \mathbf{X}_i \tag{1}$$

where m_i is the mass of the segment, $\mathbf{F}_i^h$ the hydrodynamic force, $\mathbf{F}_i^w$ is the sum of body forces (e.g. gravity), $\mathbf{f}_{ij}^{con}$ is the particle interaction force exerted on segment i by segment j of the same or other fibre, $\mathbf{f}_i^{wall}$ is the wall contact force, and $\mathbf{X}_i$ and $\mathbf{X}_{i+1}$ are the constraint forces in joints i and i+1, respectively. $\mathbf{X}_1 = \mathbf{X}_{N_{seg}+1} = \mathbf{0}$ since joints 1 and N_{seg}+1 are virtual ones.

Conservation of angular momentum on segment i is given as follows:

$$\frac{\partial}{\partial t}\left(\mathbf{I}_i \cdot \boldsymbol{\omega}_i\right) = \mathbf{T}_i^h + \sum_j \mathbf{t}_{ij}^{con} + \mathbf{t}_i^{wall} - \mathbf{Y}_{i+1} + \mathbf{Y}_i + \frac{l_i}{2}\mathbf{z}_i \times \mathbf{X}_i + \left(-\frac{l_i}{2}\mathbf{z}_i\right) \times \left(-\mathbf{X}_i\right) \tag{2}$$

where $\mathbf{I}_i$ is the inertia tensor with respect to Γ, $\boldsymbol{\omega}_i$ is the angular velocity, $\mathbf{T}_i^h$ is the hydrodynamic torque, $\mathbf{t}_{ij}^{con}$ the torque created as a result of fibre-fibre collision, $\mathbf{t}_i^{wall}$ is the torque caused by the wall

contact, $\mathbf{Y}_i$ is the sum of bending and twisting torques in joint *i*. By analogy to the constraint force $\mathbf{Y}_1 = \mathbf{Y}_{N_{seg}+1} = \mathbf{0}$ is kept for end segments.

2.2. Fibre model in present study

In the present paper the following conditions have been assumed:

- the suspending fluid is Newtonian;
- the Brownian motion is neglected;
- the velocity field is not affected by the motion of fibres, i.e. so-called one-way coupling is applied;
- there is no fibre-fibre or fibre-wall contact;
- the body force is neglected;
- fibres are inextensible;
- sphere is used to approximate an individual fibre segment.

Particle inertia may be approximated using the most recently calculated value of segment velocity. Using this one may obtain:

$$\dot{\mathbf{r}}_i = \dot{\mathbf{r}}_{i,t-\Delta t} + \frac{m_i}{\Delta t}\left(\mathbf{F}_i^h - \mathbf{X}_{i+1} + \mathbf{X}_i\right) \tag{3}$$

where Δt stands for the time interval. In order to simplify the notation, for quantities other than present, the time is explicitly indicated. For all quantities corresponding to current time step it is not specified.

Left hand side of Eq. (2) may be rewritten as follows:

$$\frac{\partial}{\partial t}\left(\mathbf{I}_i \cdot \boldsymbol{\omega}_i\right) = \dot{\mathbf{I}}_i \cdot \boldsymbol{\omega}_i + \mathbf{I}_i \cdot \dot{\boldsymbol{\omega}}_i \approx \frac{\mathbf{I}_i - \mathbf{I}_{i,t-\Delta t}}{\Delta t} \cdot \boldsymbol{\omega}_i + \frac{\mathbf{I}_i}{\Delta t}\left(\boldsymbol{\omega}_i - \boldsymbol{\omega}_{i,t-\Delta t}\right) \tag{4}$$

thus after variable grouping and manipulation Eq. (2) reduces to:

$$\boldsymbol{\omega}_i = \mathbf{A}_i^{-1} \cdot \left(\mathbf{B}_i + \mathbf{T}_i^h - \mathbf{Y}_{i+1} + \mathbf{Y}_i + \frac{l_i}{2}\mathbf{z}_i \times \mathbf{X}_i + \left(-\frac{l_i}{2}\mathbf{z}_i\right) \times \left(-\mathbf{X}_i\right)\right) \tag{5}$$

where $\mathbf{A}_i = \mathbf{I}_{i,t-\Delta t} + \frac{1}{\Delta t}\mathbf{I}_i$ and $\mathbf{B}_i = \frac{1}{\Delta t}\mathbf{I}_i \cdot \left(-\boldsymbol{\omega}_{i,t-\Delta t}\right)$.

Hydrodynamic force on segment *i* is given by the following expression:

$$\mathbf{F}_i^h = \mathbf{C}_i \cdot \left(\mathbf{u}_i^f - \dot{\mathbf{r}}_i\right) \tag{6}$$

where $\mathbf{u}_i^f$ is the ambient velocity at the segment centre-of-mass and $\mathbf{C}_i$ – the hydrodynamic resistance tensor which includes an expression for the drag coefficient in the following form:

$$C_D = a_1 + \frac{a_2}{Re} + \frac{a_3}{Re^2} \tag{7}$$

where a_1, a_2 and a_3 are constants given by Morsi and Alexander (1972) that apply to smooth spherical particles for any *Re* number. It should be pointed out that hydrodynamic force determined according to Eq. (6) does not take into account flow disturbance caused by neighbouring segments. However, this effect is not considered in other papers dealing with this same topic (see e.g. Lindström and Uesaka, 2008; Sasic and Almstedt, 2010), as it is believed to be of minor importance when compared to other forces.

Bending torque is applied when a chain deforms from its equilibrium shape. Assuming elastic bending theory the bending torque at joint i is:

$$\mathbf{Y}_i = -k_b \alpha_i \tag{8}$$

where k_b is the bending constant proportional to EI/d (E - elasticity modulus) and α_i is the bending angle, i.e. directional misalignment of two neighbouring segments.

In order to maintain fibre integrity an adequate equation has been added to the conservation system. The application of holonomic constraints at fibre joints implies that fibre segments are kept coupled during simulation. The constraint equation for i^{th} joint is as follows:

$$f(\mathbf{r}_i, \mathbf{z}_i, t) = \mathbf{r}_i + \frac{l_i}{2}\mathbf{z}_i - \left(\mathbf{r}_{i+1} + \frac{l_{i+1}}{2}\mathbf{z}_{i+1}\right) = \mathbf{0} \tag{9}$$

as illustrated in Fig 4.

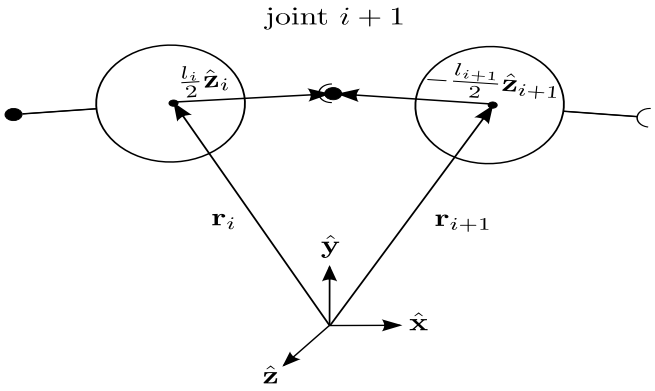

Fig. 4. The inextensibility constraint makes ball and socket joints from adjacent segments coincide

Taking time derivative of Eq. (9) one may obtain a connectivity equation which states that translational velocity of the contact point of neighbouring segments is always the same:

$$\dot{\mathbf{r}}_i - \dot{\mathbf{r}}_{i+1} + \frac{l_i}{2}\boldsymbol{\omega}_i \times \mathbf{z}_i + \frac{l_{i+1}}{2}\boldsymbol{\omega}_{i+1} \times = \mathbf{0} \tag{10}$$

where for any segment $\dot{\mathbf{z}}_i = \boldsymbol{\omega}_i \times \mathbf{z}_i$. Applying Eq. (3) and (5) to (10) leads to the equation for internal constraint in the following form:

$$\mathbf{D}_i \cdot \mathbf{X}_i + \mathbf{E}_i \cdot \mathbf{X}_{i+1} + \mathbf{F}_i \cdot \mathbf{X}_{i+2} = \mathbf{G}_i \tag{11}$$

Writing Eq. (11) for every fibre segment and making an assumption that internal forces at fibre ends are free, one may solve $N_{seg}-1$ unknown internal constraints. They can be then used to solve translational and angular velocities of each segment at corresponding time using an appropriate time integration scheme.

2.3. Calculation procedure

The numerical algorithm for solving fibre motion is composed of several steps. Starting from an initial condition calculations are carried out in the following order:

1. Initialisation of fibre configuration at time $t = 0$ - reading the fibre parameters, placing fibre segments at given positions, reading the velocity field previously calculated by CFD solver.
2. Calculation of the hydrodynamic friction forces $\mathbf{F}_i^h$ and torques $\mathbf{T}_i^h$, bending torques $\mathbf{Y}_i$ and inertia tensor $\mathbf{I}_i$ from Eqs. (3)-(5) for every fibre segment at time t.
3. Solving the internal constraint forces ($\mathbf{X}_i$) from Eq. (11) at time t.
4. Updating the fibre translation and angular velocities ($\dot{\mathbf{r}}_{i,t+\Delta t}$ and $\boldsymbol{\omega}_{i,t+\Delta t}$) as well as the centre-of-mass position $\mathbf{r}_{i,t+\Delta t}$ of every fibre segment with the explicit Euler method.
5. Calculation of the new orientation vector of every fibre segment with the following formula:

$$\mathbf{z}_{i,t+\Delta t} = \frac{\mathbf{z}_i + (\boldsymbol{\omega}_i \times \mathbf{z}_i)\Delta t}{\left|\mathbf{z}_i + (\boldsymbol{\omega}_i \times \mathbf{z}_i)\Delta t\right|} \tag{12}$$

6. Repeating steps from (2) to (5) until $t < t_{max}$.

3. FLOW CONFIGURATION

The present paper deals with the flow of a very dilute (i.e. no fibre-fibre contact) fibre suspension in a papermachine headbox. As a reference the results of an experimental study of Niskanen et al. (2011) were used. In order to investigate the flow experimentally a laboratory-scale headbox has been built (see Fig. 5). Highly turbulent flow was created upstream of the channel inlet by the bundle of tubes with sudden expansion (backward facing step configuration). Inlet height is 85 mm and outlet height is 13.5 mm which makes the contraction ratio equal to 6.3:1. The convergent section is 700 mm long and 120 mm wide. The experimental setup consists of a previously described channel and a water/suspension loop capable of producing a desired turbulence level. Particle Image Velocimetry (PIV) technique was used to obtain velocity maps at eight streamwise positions. Fibre orientation statistics was determined with a high speed camera coupled with PC.

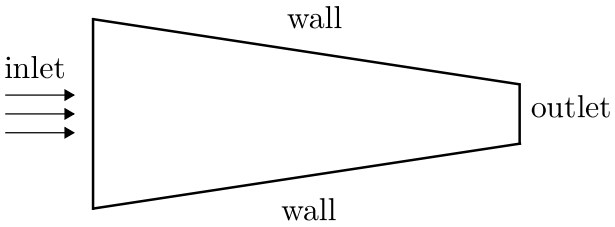

Fig. 5. A schematic drawing representing geometry of the analysed headbox

Taking into account nearly two-dimensional character of the flow in the headbox (relatively large width in comparison to the height of the channel) it was decided to apply 2-dimensional model of the flow. The geometry and computational grid were created by means of ANSYS GAMBIT commercial code. The mesh is of a structured type and due to boundary layer and high shear rates foreseen in the flow, an appropriate cell distribution has been applied - see Fig. 6.

A series of grids of different sizes (20k, 40k, 60k, 85k and 105k) was analysed to come up with an optimal grid of appr. 85 000 cells ensuring grid independent solution. The flow field was solved with a commercial CFD software ANSYS FLUENT. The effect of non-uniform flow field (due to turbulence generator not considered in the geometry) has been included by means of an adequate boundary condition at the inlet to the domain. The implementation of the mean velocity profile as well as turbulent kinetic energy and its dissipation was done with the help of the user defined function (UDF) - a subroutine linked to the solver. Turbulence was modelled with Reynolds Stress Model (RSM). Pressure and momentum equations have been discretised with second order accuracy schemes.

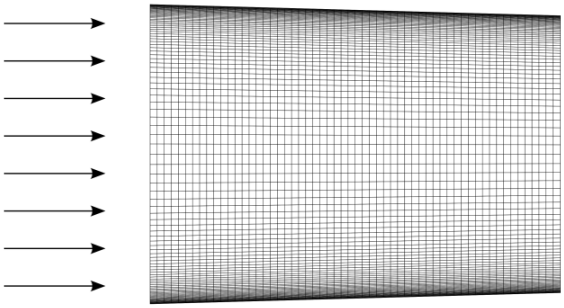

Fig. 6. Computational mesh in the inlet region

4. RESULTS AND DISCUSSION

4.1. Model validation

Correctness and relevance of the model have been validated by performing test calculations for single fibres both for rigid and flexible ones. At first, only rigid fibres were taken into consideration. Jeffery (1922) predicted theoretically that the major axis of a prolate spheroid of aspect ratio a_e should exhibit periodic rotation while immersed in a sheared viscous fluid. Period of so-called Jeffery's orbit is given by the following equation:

$$T = 2\pi(a_e + 1/a_e)\dot{\gamma} \tag{13}$$

where $\dot{\gamma}$ is a shear rate.

Verification of the proposed model was done by the comparison of normalised rotation period $T\dot{\gamma}$ as a function of fibre aspect ratio with Eq. (13) as well as with available literature data, including a model of Ross and Klingenberg (1997) (fibres with spherical elements) and experimental results for rigid cylinders reported by Goldsmith and Mason (1967).

Fibre was initially aligned along the y axis (see Fig. 7a) in such a way that the centre of mass of the fibre was located in an origin of the coordinate system. A simple shear flow $U = [y\dot{\gamma};0;0]$ was applied resulting in a rotational motion of fibre as shown in Fig. 7b.

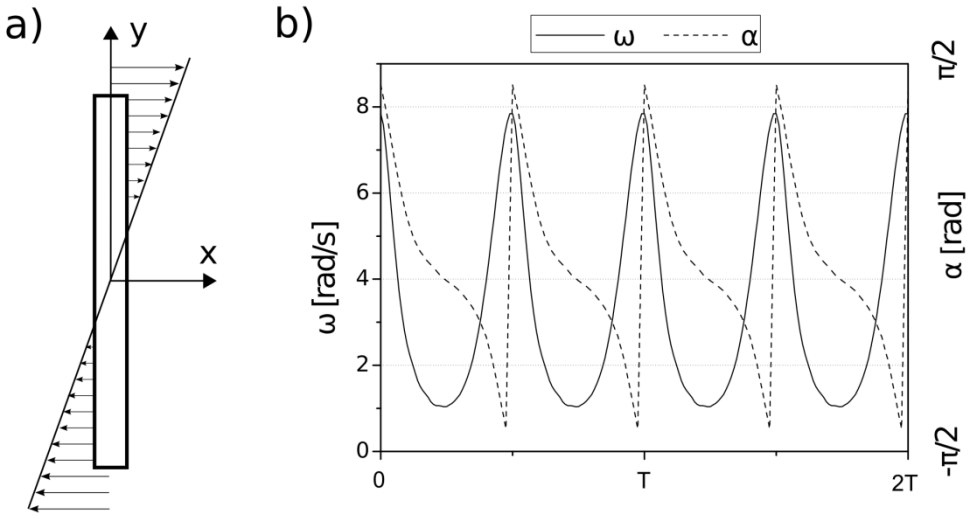

Fig. 7. a) Fibre initial position in a simple shear flow; b) Time variation of fibre angular velocity ω and orientation angle α

Instantaneous values of angular velocity as well as orientation angle α (defined in Fig. 7a) are dependent on current fibre orientation, i.e. alignment with respect to the flow field. The lowest velocity is observed when fibre is aligned with the flow direction while the highest one occurs otherwise, i.e. $\alpha = \pm\pi/2$.

It can be easily found (see Figure 8) that the developed model indicates full consistency with the previously mentioned source literature. The $T\dot{\gamma}$ distribution obtained in the present study agrees very well with data of Ross and Klingenberg (1997) who were using an identical fibre model (sphere as a fibre segment). The observed deviations from two remaining sets of data may be explained by different element shapes, i.e. ellipsoids for Jeffery (1922) and cylinders for experiment done by Goldsmith and Mason (1967).

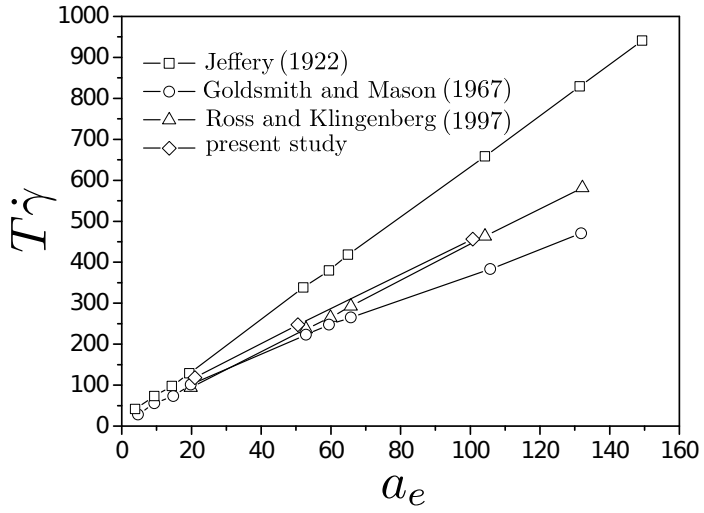

Fig. 8. Comparison of simulated, theoretical and measured periods of rotation for rigid fibres as a function of aspect ratio in a simple shear flow

Following the tests for rigid fibres a series of simulations was conducted for flexible ones. The fibre model allows to set the bending stiffness at a desired value and in this way to study the influence of fibre type on its behaviour. Figure 9 presents the sample evolution of fibre deformation in a simple shear flow. The consecutive images are reasonable and indicate full consistency with reference results of Ross and Klingenberg (1997). This confirms that the developed fibre model is capable of simulating its deformation dynamics in a realistic way.

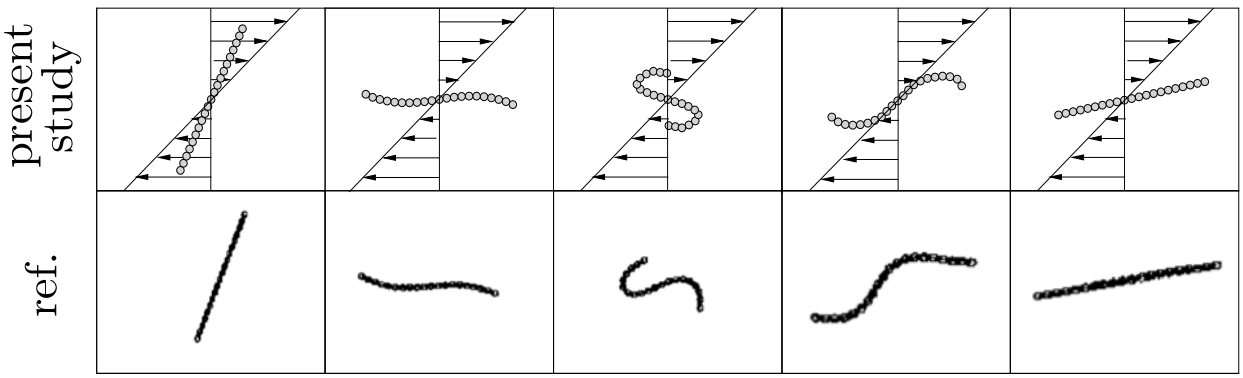

Fig. 9. Evolution of the flexible fibre deformation in simple shear flow compared with results obtained by Ross and Klingenberg (1997)

4.2. Flow dynamics in 2D headbox

Fibre motion in a convergent section of the papermachine headbox was resolved in a two-step procedure. The geometry and the flow conditions of a simplified headbox described in section 2.2 were used to calculate velocity field. Fibre dynamics was then analysed using the in-house code with the previously determined velocity field as an input.

The flow rate was set at the level 0.024 m^3/s. The flow Reynolds number at the channel outlet was equal to $0.97 \cdot 10^5$ defined on the maximum streamwise velocity $U_{x,max}(x = L)$, the local height $h(x)$ of the channel and the kinematic viscosity of the fluid v. In Figure 10 the local streamwise velocity is plotted as a function of non-dimensional longitudinal coordinate $x^* = x/L$, where L is the channel length. Due to channel geometry fluid accelerates continuously which is especially evident when approaching the headbox outlet.

According to Olson et al. (2004) and Ullmar (1998) the strain rate, defined as $\partial U_x/\partial x$, is a dominant term affecting fibre orientation in a streamwise elongational flow. That is why the strain rate distribution is also presented in Fig. 10.

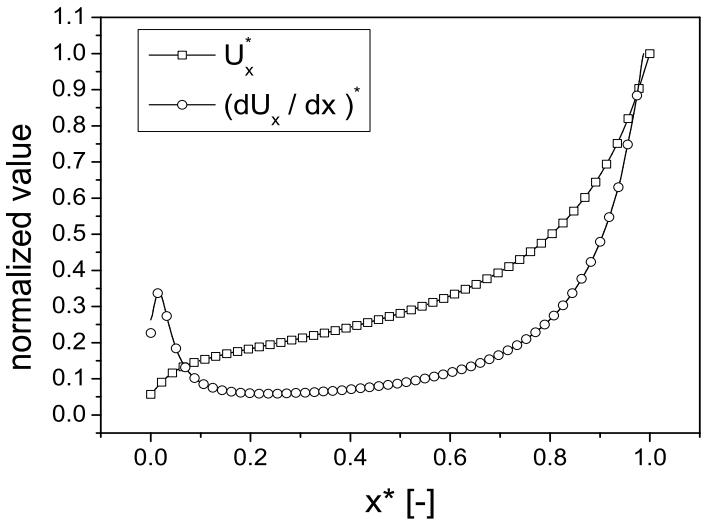

Fig. 10. Longitudinal profiles of mean velocity and velocity gradient at the channel centre line

Velocity gradients as well as streamwise velocity are presented in a normalised way, i.e. both quantities are divided by their values at the outlet cross-section. One may notice an increased level of strain rate just downstream the channel inlet, which may be explained by a non-uniform feed of the headbox by distributing pipes. A very strong elevation of $\partial U_x/\partial x$ is observed in the outlet part which is much more pronounced than the increase of velocity at this channel section. The remaining velocity gradients are negligible when compared to $\partial U_x/\partial x$.

The velocity profiles shown in Fig. 11 are presented in a non-dimensional form, i.e. velocity U_x is scaled by maximum velocity at the outlet producing U^* while non-dimensional spanwise coordinate y^* is defined as a ratio of distance from the channel centre-line and channel inlet half-height $h_{in}/2$. Profiles which are close to the inlet are deformed due to the presence of turbulence generator. However, at a certain distance downstream the channel inlet flow disturbance vanishes and velocity profiles become typical for a linear contraction channel.

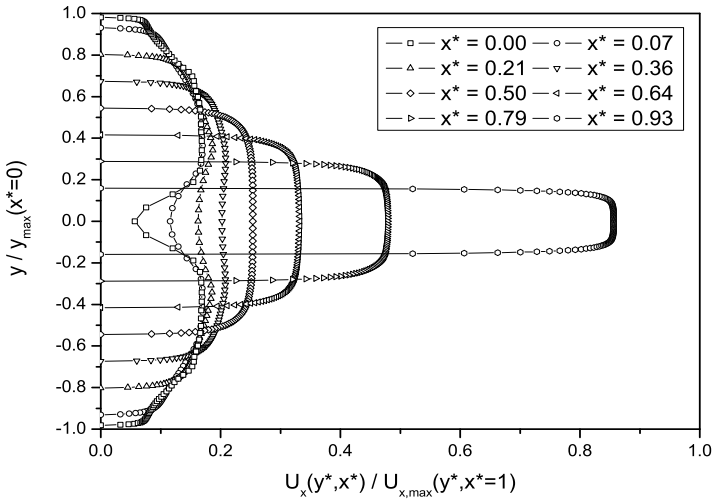

Fig. 11. Evolution of streamwise velocity profiles along the channel

4.3. Rigid fibre simulation

Rigid fibre behaviour was obtained by setting the bending constant at a relatively high level, in principle fibre is rigid when $k_b \rightarrow \infty$, but in order to avoid convergence problems the value of k was chosen iteratively by observing changes of fibre contour. In total the motion of 198 fibres was investigated. In order to save computational time the motion of fibres was analysed starting from the cross-section x^*= 4/7, where the acceleration of flow becomes influential on the fibre orientation. The selection of this cross-section was made on the basis of some test calculations. Fibres were initially placed in several spanwise positions y_0 starting from the axis towards the wall. From each transverse position fibres aligned with 18 different initial orientation angles α_{init} were released resulting in uniform probability distribution function $\Psi(\alpha)=1/\pi$ of fibre orientation (198 sample population). As the fibre-wall contact model had not been implemented yet it was necessary to reject from the population those fibres for which contact with the wall had been detected. Two lengths of fibre have been investigated, namely 1 mm and 2 mm, both of a diameter equal to 25 μm.

Fibre motion in a simple 2D convergent channel without turbulent fluctuations is driven by velocity gradients both in streamwise and spanwise directions. The rate of change of orientation is clearly affected by the initial transverse position and increases with a reduction of the distance from the wall. Sample orientation evolutions for fibres inclined at the fixed angle of 50 deg released from different spanwise positions are shown in Fig. 12.

A change of the initial orientation is observed in the region where velocity gradient becomes significant (see Fig. 10). This justifies the assumption about the choice of fibre release position. The fibre flowing in near wall region (affected by strong spanwise velocity gradient) starts to change the orientation angle at the position x^* = 0.8 and rotates in anti-clockwise direction whereas fibre suspended in the core flow (y_0^* = 0.08 – uniform velocity profile) rotates in opposite direction and keeps unchanged orientation practically to the closest vicinity of the outlet.

The available database of fibre dynamics allowed to determine probability density functions of the fibre orientation angle in the channel, in particular at its outlet (x^*= 1). Exact pdf values for 1 mm fibre length are plotted in Fig. 13 using bars. In order to obtain a smooth distribution the original histogram was approximated by the three-parameter Gaussian curve (classical distribution including offset) which is drawn with triangles.

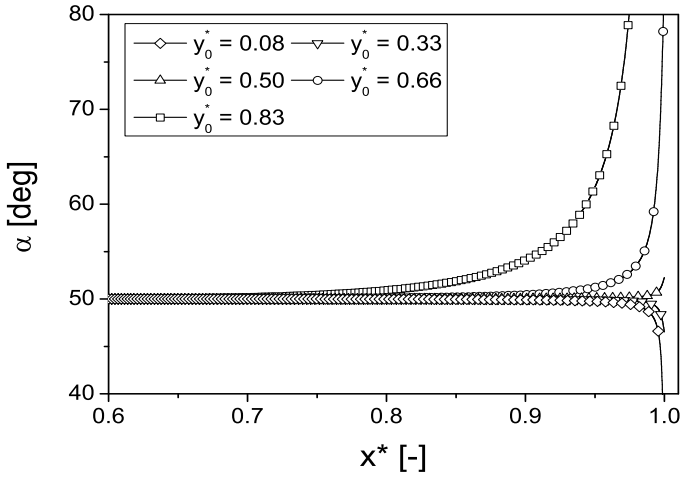

Fig. 12. Sample orientation evolutions of fibres released from different spanwise positions

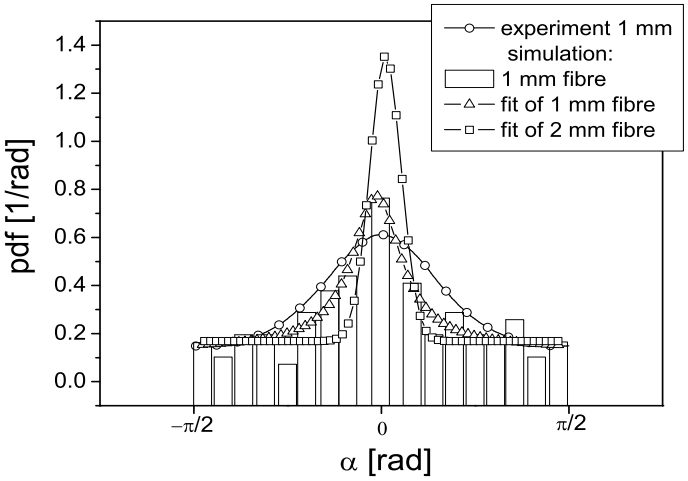

Fig. 13. Probability density function of fibre orientation at x^*= 1

While a qualitative agreement of experimental and simulation results is observed, one should notice quantitative discrepancies. These may be explained by the negligence of turbulent fluctuations in the calculation of hydrodynamic interactions. According to Sasic and Almstedt (2010) turbulent diffusion influences fibre dynamics leading statistically to less pronounced peak of the pdf of fibre orientation. Moreover, a simplification of the flow to two dimensions, i.e. negligence of flow component in z-direction, elimination of fibres in close proximity of the wall may contribute to the deviation of the calculation results from experimental distribution. One could expect that both of the above mentioned influences should lead to a less anisotropic distribution of fibre orientation (defined as $\Psi(0)/\Psi(\pi/2)$). At the next step, simulations for longer (2mm) fibres were conducted. As can be seen from Fig. 13 the longer the fibre the stronger the anisotropy of FOPD. This tendency was also observed in an experiment of Putkiranta et al. (1997). Statistically, the longer the fibre the higher is the chance the fibre's end is immersed in a near-wall region, contributing mostly to the fibre alignment effect.

4.4. Flexible fibre simulation

Fibres encountered in practical situations may have extremely various properties. In papermaking the origin of fibre as well as different stock preparation operations (chemical or mechanical) may strongly

affect fibre properties leading among others to an extremely wide range of fibre bending stiffness. That is why the analysis of deformable fibres is of great practical importance.

As previously stated, the model developed in the present paper is capable of simulating the motion of any deformable fibre. In order to show the influence of the fibre flexibility on its dynamical behaviour in a headbox, a series of simulations for an arbitrarily chosen stiffness (corresponding to the beaten pine fibres) was carried out for the same initial and flow conditions as for the rigid fibres simulation described in section 4.3.

Flexible fibre shapes presenting orientation evolution for near-outlet channel region, where the rate of strain is sufficiently pronounced to influence fibre dynamics, are shown in Figure 14. For reference the snapshots of rigid fibre at the same time instants were superimposed.

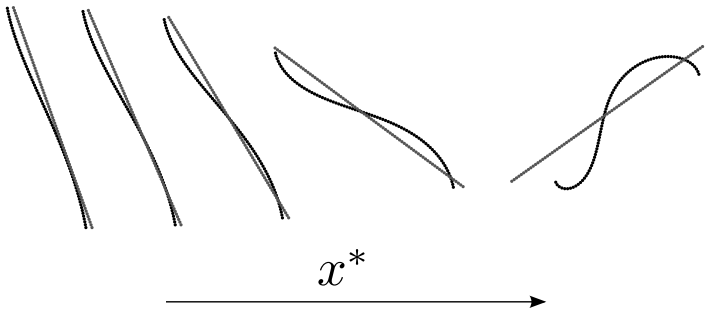

Fig. 14. Shape and mean orientation of flexible and rigid fibres during their motion in a close neighbourhood of the channel outlet

As can be seen fibre flexibility does not particularly influence mean fibre orientation and position in the flow. Fibre flexibility leads to its deformation which starts to be visible at the beginning of the region under analysis and becomes more and more pronounced while approaching the channel outlet. Although mean fibre orientation for flexible fibre is the same as for rigid one, its contour is important in terms of flock (fibre agglomerate) formation and final product properties. Qualitatively a similar behaviour was observed for fibres released at different spanwise locations and initially characterised by different orientation angles. It should be stressed that the above observations refer only to the case of dilute suspension, i.e. when fibre is affected by neither other fibres nor flow boundaries.

5. CONCLUSIONS

In this paper, the Lagrangian method (particle-level method) was employed to simulate dynamics of rigid and flexible fibres suspended in flow. A single fibre was modelled as a chain of segments, i.e. spheres connected by ball and socket joints. Stiffness of the fibre was controlled by varying resistance at fibre joints. Appropriate expressions for hydrodynamic force have been adopted from the literature for a wide range of Reynolds numbers. Translational and rotational equations of motion were solved for every segment after calculating internal constraint forces responsible for maintaining fibre integrity.

The model was firstly tested in a simple shear flow to demonstrate the methodology used in the present study was correct - rigid fibres reproduced well known dynamic behaviour, and their period of rotation agreed well with Jeffery's theory.

The model was then applied to simulate fibre motion in a papermachine headbox. The aim of the study was to analyse fibre orientation in a converging channel. The fibre orientation probability distribution was constructed taking into account the motion of 198 fibres initiated with random orientation and spanwise position. The results compared to the experimental data showed qualitative agreement proving the model's relevance to describe fibre dynamics. However, some quantitative discrepancies

between the simulations and the experimental results which may be explained by the model's simplifications (negligence of turbulent fluctuations on fibre motion, two-dimensionality of the flow as well as no wall contact model) were observed. Longer fibres were found to be more sensitive to the flow field - their orientation distribution is more anisotropic. Although the sample test simulation of flexible fibres motion showed that their mean orientation angle was more less the same as that for rigid fibres, their shapes may influence other paper properties and should be taken into account in analysing fibre flow phenomena.

In practical applications the consistency of fibre suspension may vary from 0.05% even up to 8%, thus fibre-fibre and fibre-wall contacts should be included when modelling the phenomenon. A high consistency additionally means that fibres as discrete objects influence fluid motion thus a corresponding term in the momentum equation should appear. The model developed in the present paper is foreseen to be extended in order to include the above mentioned aspects of fibre suspension flow.

SYMBOLS

N_{seg}	number of segments in a fibre
$\mathbf{r}_i$	centre-of-mass position vector, m
$\dot{\mathbf{r}}_i$	translational velocity vector, m/s
$\mathbf{z}_i$	orientation of fibre segment vector, m
Γ	global right-hand coordinate system
Γ_i	local right-hand coordinate system
$\mathbf{F}_i^h$	hydrodynamic force vector, N
$\mathbf{F}_i^w$	sum of body forces vector, N
$\mathbf{f}_{ij}^{con}$	particle interaction force vector, N
$\mathbf{f}_i^{wall}$	wall contact force vector, N
$\mathbf{X}_i$	constraint force vector, N
$\mathbf{I}_i$	inertia tensor with respect to Γ, kgm^2
$\boldsymbol{\omega}_i$	angular velocity vector, rad/s
$\mathbf{T}_i^h$	hydrodynamic torque vector, Nm
$\mathbf{t}_{ij}^{con}$	torque vector created as a result of fibre-fibre collision, Nm
$\mathbf{t}_i^{wall}$	torque vector caused by the wall contact, Nm
$\mathbf{Y}_i$	vector containing sum of bending and twisting torques, Nm
$\mathbf{C}_i$	hydrodynamic resistance tensor, kg/s
C_D	drag coefficient, -
k_b	bending constant, Nm/rad
E	elasticity modulus, GPa
T	orbit period, s
$\dot{\gamma}$	shear rate, 1/s
U	fluid velocity, m/s
Ψ	fibre orientation probability distribution (FOPD),-

Subscripts

i	segment number

REFERENCES

Batchelor G. K., 1962. Slender-body theory for particles of arbitrary cross-section in Stokes flow. *J. Fluid Mech*., 44, 419–440. DOI: 1017/S002211207000191X.

Brenner H., 1964. The Stokes resistance of an arbitrary particle-IV Arbitrary fields of flow. *J. Fluid Mech.*, 19, 702–727. DOI: 10.1016/0009-2509(64)85084-3.

Bretherton F.P., 1962. The motion of rigid particles in a shear flow at low Reynolds number. *J. Fluid Mech.*, 14, 284–304. DOI: 10.1017/S002211206200124X.

Goldsmith H.L. and Mason S.G., 1967. The microrheology of dispersions. In: Eirich F.R. (Ed.). *Rheology: Theory and applications*. New York, Vol. 4, 85-250.

Jeffery G.B., 1922. The motion of ellipsoidal particles immersed in a viscous flow. *Proc. R. Soc. A*, 102, 161–179.

Jetsu P., Kellomaäki M., Karema H., Salmela J., Lappalainen T., Piirto M., 2001. Coherent structures of suspension flow and their inheritance in paper. In: *12th Fundamental Research Symposium*, Oxford, UK, September 2001.

Leppanen T., 2007. *Effect of fiber orientation on cockling of paper*. PhD Thesis. University of Kuopio, Finland.

Lindström S.B., Uesaka T., 2008. Particle-level simulation of forming of the fibre net- work in papermaking. *Int. J. Eng. Sci*., 46, 858–876. DOI: 10.1016/j.ijengsci.2008.03.008.

Morsi S.A., Alexander A.J., 1972. An investigation of particle trajectories in two phase flow systems. *J. Fluid Mech*., 55, 193–208. DOI: 10.1017/S0022112072001806.

Niskanen H., Eloranta H., Hämälainen J.P., 2011. On the orientation of flexible fibres in a contracting channel flow. *Int. J. Multiphase Flow*, 37, 336–345. DOI: 10.1016/j.ijmultiphaseflow.2010.11.006.

Olson J.A., Frigaard I., Chan C., Hämälainen J.P., 2004. Fiber orientation modelling applied to contracting flows related to papermaking: The one-dimensional headbox. *Int. J. Multiphase Flow*, 30, 51–66. DOI: 10.1016/j.ijmultiphaseflow.2003.10.006.

Putkiranta M., Eloranta H., Pärssinen T., Saarenrinne P., 2009. Evolution of the fibre orientation distribution in streamwise elongational flow. In: Madetoja E., Niskanen H., Hämälainen J.P. (Eds.), *Papermaking Research Symposium*. Kuopio, Finland, 1–4 June, 2009.

Ross R.F., Klingenberg D.J., 1997. Dynamic simulation of flexible fibers composed of linked rigid bodies. *J. Chem. Phys.,* 106, 2949–2960. DOI: 10.1063/1.473067.

Sasic S., Almstedt A.E., 2010. Dynamics of fibres in a turbulent flow field - A Novel particle-level simulation technique. *Int. J. Heat Fluid Flow*, 31, 1058–1064. DOI: 10.1016/j.ijheatfluidflow.2010.05.009.

Schmid C.F., Klingenberg D.J., Scott C.T., 2000. Simulation of fibre flocculation: Effect of fibre properties and inter-fibre friction. *J. Rheol*., 44, 781–809. DOI: 10.1122/1.551116.

Ullmar M., 1998. *On fibre orientation mechanisms in a headbox nozzle*. PhD Thesis. Royal Institute of Technology, Stockholm, Sweden.

Yamamoto S., Matsuoka T., 1993. A method for dynamic simulation of rigid and flexible fibers in a flow field. *J. Chem. Phys.*, 98, 644–650. DOI: 10.1063/1.464607.

Yamamoto S., Matsuoka T., 1994. Viscosity of dilute suspension of rodlike particles: A numerical simulation method. *J. Chem. Phys*., 100, 3317–3324. DOI: 10.1063/1.466423.

Yamamoto S., Matsuoka T., 1995. Dynamics simulation of fiber suspension in shear flow. *J. Chem. Phys*., 102, 2254–2260. DOI: 10.1063/1.468746.

Yamamoto S., Matsuoka T., 1999. Dynamics simulation of rod-like and plat-like particle dispersed system. *Comp. Mat. Sci*., 102, 169–176. DOI: 10.1016/S0927-0256(98)00103-7.

Received 26 April 2012
Received in revised form 17 October 2012
Accepted 30 October 2012